Polymer Journal (2014) 46, 617–622

www.nature.com/pj

ORIGINAL ARTICLE

# Chain-length dependence of polyion complex architecture bearing phosphobetaine block explored using SAXS and FFF-MALS

Shunsuke Sakamoto[1,2], Yusuke Sanada[1,2], Mizuha Sakashita[1,2], Koichi Nishina[1], Keita Nakai[3], Shin-ichi Yusa[3] and Kazuo Sakurai[1,2]

**Synchrotron small-angle X-ray scattering (SAXS) was measured from aqueous solutions of polyion complexes (PICs), which were prepared by mixing oppositely charged diblock copolymers MAPTAC-*b*-PMPC and AMPS-*b*-PMPC. MAPTAC represents polycationic (3-(methacryloylamino)propyl)trimethylammonium chloride, AMPS represents polyanionic sodium 2-(acrylamido)-2-methylpropanesulfonate and PMPC represents hydrophilic poly-zwitterion (2-(methacryloyloxy)ethyl phosphorylcholine). The degrees of polymerization of MAPTAC and AMPS were selected to be the same for each complex, and the ratio ($R_p$) of the polymerization degree for the cationic to neutral chains was changed from 0.27 to 9.5. The aggregation number ($N_{agg}$) of PIC was determined with light scattering combined with field-flow fractionation (FFF). The inner structures of PIC were determined by analyzing SAXS with the core-corona model. When the MPC chain was much longer than the charged ones ($R_p = 0.27$), a star-like spherical conformation was formed. With an increase of $R_p$, $N_{agg}$ increased, while the spherical form was maintained up to $R_p = 1.0$. When $R_p = 4.7$ and 9.5, the PIC became a worm-like cylinder and vesicle, respectively. Based on the determined structural parameters and aggregation numbers, the index to describe how the tethered PMPC chains were crowded on the shell was determined. It was observed that the crowding parameter was much smaller than that of poly(ethylene glycol in spherical core-shell polymeric micelles.**
*Polymer Journal* (2014) **46,** 617–622; doi:10.1038/pj.2014.25; published online 28 May 2014

**Keywords:** polyion complex; polymer micelle; synchrotron small-angle X-ray scattering

## INTRODUCTION

Mixing two oppositely charged homo-polyelectrolytes results in polyion complexes (PICS), and their isoelectric mixing normally results in water-incompatible aggregates, which gradually coagulate to form larger aggregates and eventually precipitates.[1,2] Harada and Kataoka[3] reported that when oppositely charged diblock copolymers H-A and H-C are mixed, where H, A and C represent non-ionic hydrophilic, anionic and cationic chains, the A and C blocks form a water-incompatible complex and the hydrophilic H chains cover to conceal the A/C complex from water. Thus, secondary coagulation is drastically reduced. In other words, the isoelectric H-A/H-C mixtures take a core-shell type micelle. In contrast to the case of classical PICs, the aqueous solutions dispersing these micelles are quite stable and their size shows an extremely narrow distribution. Presumably, their micellar structures are determined by a combination of the polyions and hydrophilic chain lengths and their chemical structures. This type of PIC micelles is denoted by PIC micelles in distinction from classical PICs prepared from homopolymers. It is interesting that the PIC micellar formation is quite similar to that of amphiphilic block copolymers.[4]

One of the major applications of PIC micelles is drug-delivery systems.[5] In most cases, poly(ethylene glycol) (PEG) is used as the hydrophilic block with a similar purpose, with micelles made from amphiphilic block copolymers, that is, biocompatibility and enhancement of blood circulation.[6] Thus, PEG has been used in many systems in biological applications and the coined term of 'pegylation' has become popular. Recently, several groups have emphasized a drawback of PEG: it can induce an immunological response for frequent dosing. This phenomena was first reported by Ishida *et al.*[7,8] for pegylated liposomes. According to these authors, pegylated liposome was rapidly cleared from the blood and accumulated in the liver when injected twice in the same rat or mouse at several-day intervals, called the 'accelerated blood clearance phenomenon'. As an alternative, a photophilic polymer bearing a zwitterion as a side chain such as poly poly(2-(methacryloyloxy) ethylphosphorylcholine) (pMPC) has been synthesized using the reversible addition-fragmentation chain transfer radical polymerization method.[9] According to Morisaku *et al.*,[10] each MPC repeating unit is associated with ~24 water molecules, whose number is much

[1]Department of Chemistry and Biochemistry, University of Kitakyushu, Fukuoka, Japan; [2]Structural Materials Science Laboratory SPring-8 Center, RIKEN Harima Institute Research, Hyogo, Japan and [3]Department of Materials Science and Chemistry, Graduate School of Engineering, University of Hyogo, Hyogo, Japan
Correspondence: Professor K Sakurai, Department of Chemistry and Biochemistry, University of Kitakyushu, 1-1 Hibikino, Wakamatsu, Kitakyushu, Fukuoka 808-0135, Japan.
E-mail: sakurai@kitakyu-u.ac.jp
Received 4 February 2014; revised 13 March 2014; accepted 14 March 2014; published online 28 May 2014

larger than that of PEG, which explains why pMPC is more biocompatible than PEG. In fact, biological systems use zwitterion-type phospholipids in which an anionic phosphate group is combined with a cationic choline. These phospholipids are the major component of all cell membranes, and these zwitterions form the biological surface of cells.

Recently, we synthesized a series of diblock copolymers consisting of an MPC block and either a cationic MAPTAC or anionic AMPS block using reversible addition-fragmentation chain transfer-controlled radical polymerization. Here, MAPTAC and AMPS represent poly(3-(methacryloylamino)propyl)trimethylammonium chloride and poly(2-(acrylamido)-2-methylpropanesulfonate), respectively (Figure 1). The mixing of aqueous solutions of oppositely charged diblock copolymers, pMPC-*b*-pMAPTAC and pMPC-*b*-pAMPS, led to the spontaneous formation of PIC micelles.[11] The aim of this study is to characterize these PIC micelles using synchrotron small-angle X-ray scattering (SAXS) and multi-angle light scattering (MALS) to elucidate the details of the micellar architecture.

## EXPERIMENTAL PROCEDURE

### Materials and micelle preparation

Ten samples of pMPC-*b*-pMAPTAC or pMPC-*b*-pAMPS were newly synthesized using a pMPC-based chain-transfer agent for this study. The synthetic details are presented elsewhere.[12] The molecular characters and the sample codes used in this paper are summarized in Table 1, where P, M and A represent pMPC, pMAPTAC and pAMPS, respectively, and the following number indicates the degree of polymerization for each block. The number-averaged molecular weight was determined using $^1$H NMR.[12] PEG with a molecular weight of 400 g mol$^{-1}$ was obtained from Wako Pure Chemical Industries, Ltd (Osaka, Japan) and denoted PEG400.

The obtained pMPC-*b*-pMAPTAC and pMPC-*b*-pAMPS were dissolved separately in distilled water containing 0.1 M NaCl (the salt concentration was the same unless otherwise noted). After being left overnight at room temperature, a pMPC-*b*-pMAPTA solution was added dropwise to a pMPC-*b*-pAMP solution with stirring. The mixing ratio defined by $f = [\text{MAPTAC}]/([\text{AMPS}] + [\text{MAPTAC}])$ was 0.5 at the isoelectrical composition. We prepared five PIC samples for the present work, and the sample codes and combination of pMPC-*b*-pMAPTAC and pMPC-*b*-pAMPS are presented in Table 2. Here we introduce the ratio of the polymerization degree of the cationic to neutral chains ($R_p$), as indicated in the second column of the table.

### FFF coupled with MALS

An Eclipse 3+ separation system (Wyatt Technology Europe, Dernbach, Germany) was used as FFF, which was sequentially connected to a Dawn Heleos II multiangle static LS detector (Wyatt Technology) and an Optilab rEX DSP differential refractive index (RI) detector (Wyatt Technology) operating at a wavelength of 658 nm, in that order from the upper stream. A Wyatt channel (Eclipse 3 channel LC) was used, which had a tip-to-tip length of 17.4 cm and a nominal thickness of 250 μm and a membrane (Nadir cellulose membrane 10 kDa LC) was attached to the bottom of the channel. The specific refractive index increment ($\partial n/\partial c$) of the PIC micelles in 0.1 M NaCl aqueous solution was determined for each sample using a DRM-1021 differential refractometer (Otsuka Electronics, Osaka, Japan). The obtained value was used to determine the molar mass ($M_{FFF}$) for each fraction from the LS intensity using the Berry plots. The weight-averaged and number-averaged molar masses ($M_w$ and $M_n$) were calculated from RI and $M_{FFF}$ fractograms, assuming monodispersity for all fractions. The average aggregation number $N_{agg}$ was determined using the relation of $N_{agg} = M_w/(M_{\text{pMPC-b-pMAPTAC}} + M_{\text{pMPC-b-pANPS}})$, where $M_{\text{pMPC-b-pMAPTAC}}$ and $M_{\text{pMPC-b-pANPS}}$ are the number-averaged molecular weight indicated by each subscript.

**Table 1 Sample codes and their molecular characteristics used in this study**

| *Sample code* | $M_n$ *of pMPC* | $M_n$ *of pMAPTAC* | $M_n$ *of pAMPS* |
|---|---|---|---|
| P100M27 | $2.98 \times 10^4$ | $6.01 \times 10^3$ | — |
| P100A27 | ibid | — | $6.10 \times 10^3$ |
| P100M48 | ibid | $1.11 \times 10^4$ | — |
| P100A45 | ibid | — | $9.10 \times 10^3$ |
| P100M96 | ibid | $1.92 \times 10^4$ | — |
| P100A99 | ibid | — | $2.05 \times 10^4$ |
| P20M94 | $6.21 \times 10^3$ | $2.08 \times 10^4$ | — |
| P20A96 | ibid | — | $2.03 \times 10^4$ |
| P20M190 | ibid | $4.33 \times 10^4$ | — |
| P20A196 | ibid | — | $4.23 \times 10^4$ |

Abbreviations: pAMPS, poly (2-(acrylamido)-2-methylpropanesulfonate; pMAPTAC, poly ((3-(methacryloylamino)propyl)trimethylammonium chloride; pMPC, poly(2-(methacryloyloxy)ethylphosphorylcholine).
$M_n$: determined with $^1$H NMR.

**Table 2 Sample codes of the PICs and the molar mass, and its distribution determined using FFF-MALS in [NaCl] = 0.1 M**

| *Code* | *Combination* | $R_P$ | *dn/dc/* $cm^3 g^{-1}$ | $M_w$/ $g\,mol^{-1}$ | $M_w/M_n$ | $N_{agg}$[a] |
|---|---|---|---|---|---|---|
| C03 | P100M27 + P100A27 | 0.27 | 0.141 | $1.7 \times 10^5$ | 1.05 | 2.3 |
| C05 | P100M48 + P100A45 | 0.48 | 0.139 | $8.3 \times 10^5$ | 1.02 | 10 |
| C10 | P100M96 + P100A99 | 0.96 | 0.150 | $3.1 \times 10^6$ | 1.01 | 30 |
| C50 | P20M94 + P20A96 | 4.7 | 0.150[b] | $3.7 \times 10^6$ | 1.04 | 69 |
| C100 | P20M190 + P20A196 | 9.5 | 0.150 | $1.0 \times 10^9$ | 1.19 | $1.1 \times 10^4$ |

Abbreviations: FFF, field-flow fractionation; MALS, multi-angle light scattering; PICS, polyion complexes.
[a]Defined by $M_w/(M_{\text{pMPC-b-pMAPTAC}} + M_{\text{pMPC-b-pANPS}})$.
[b]Estimated value based on the chemical composition.

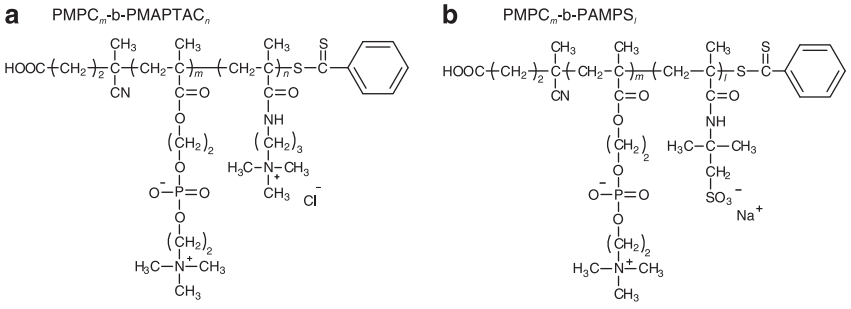


**Figure 1** The chemical structure of the cationic diblock copolymer (PMPC$_m$-b-PMAPTAC$_n$) (**a**) and the anionic diblock copolymer (PMPC$_m$-b-PAMPS$_l$) (**b**).

### Synchrotron SAXS measurements

SAXS measurements were performed at BL40B2 of SPring-8, Japan.[13] A 30 cm × 30 cm imaging plate (Rigaku R-AXIS VII, Tokyo, Japan) detector was placed at 0.75 or 1.65 m away from the sample. The wavelengths of the incident beam ($\lambda$) were 0.071 or 0.10 nm. The 0.75 and 1.65 m set-ups provided $q$ ranges of 1.0–8.0 and 0.08–2.0 $nm^{-1}$, respectively. The irradiation time was fixed at 300 s for all the measurements. A bespoke SAXS vacuum sample chamber[14] was used and the X-ray transmittance of the samples was determined with an ion chamber located in front of the sample and a Si photodiode for the X-ray (Hamamatsu Photonics S8193, Shizuoka, Japan) after the sample. We verified that no irradiation damage occurred in preliminary experiments.

As one of the strongest X-ray sources in the world was being used, we were able to obtain the scattering profiles with a large S/N even at low concentrations of 1.0 mg $ml^{-1}$ for C03, C05, C10 and C50, and 0.5 mg $ml^{-1}$ for C100. In the previous study, we confirmed that the interparticle diffraction, that is, the structural factor, was negligibly small and, thus, we considered only form factors from scattering objects at these concentrations. The fitting model and its theoretical equations are presented in the Supplementary Information.

## RESULTS AND DISCUSSION

### Determination of the aggregation number with FFF

Figure 2 presents the FFF elution fractograms recorded with LS at 90° (upper) and the concentration determined from refractive index (lower) for three NaCl concentrations ([NaCl]) of C03. The values of $M_{FFF}$ determined from MALS are plotted in the upper panel, indicating that $M_{FFF}$ of the 0.1, 0.5 and 1.0 M solutions ranged from 2 to $3 \times 10^6$, 2 to $5 \times 10^5$ and 3 to $8 \times 10^4$, respectively. Here, [NaCl] of the eluting solvent was adjusted to be the same as that of the sample solution. We injected the same amount of the sample; however, the 0.1 M solution exhibited a much larger peak area than the others. When we calculated the recovery ratio (defined by the ratio of the injected to eluted amounts of solute), the ratio for the 0.1 M solution was almost 100%, while those of the 0.5 and 1.0 M solutions were 47% and 58%, respectively, indicating that almost half of the solutes for the 0.5 and 1.0 M solutions did not come out and most likely went through the membrane filter attached to the bottom of the FFF channel during the focusing or measurement processes. These results can be interpreted as follows: at the higher [NaCl], the polyion parings in PIC were more disturbed by the ion exchange with sodium or chloride ions and, thus, the unimer/micelle equilibrium shifted to be more favorable for unimer formation. As the size of the unimer was small enough that the unimer was able to pass through the membrane filter, the recovery decreased with an increase of [NaCl]. As almost 100% recovery was attained at 0.1 M, hereinafter, we performed all the measurements at [NaCl] = 0.1 M.

According to Yusa at *et al.*,[12] dynamic LS revealed a similar ionic strength dependence as that in Figure 2 (see Supplementary Figure 1). The hydrodynamic radii thus obtained remained constant up to 0.1 M and gradually decreased, eventually reaching $<3$ nm at [NaCl] $>0.9$ M. These results indicated that in this high [NaCl], PIC micelles dissociated into unimers. These results indicated that PIC formed stable aggregates unless [NaCl] exceeded 0.15 M, which is another reason why we performed all the measurements at [NaCl] = 0.1 M.

Although the data are not shown, FFF-MALS were performed for the other samples and the calculated $M_w$, $M_w/M_n$, and $N_{agg}$ are listed in Table 2. For C03: $R_p = 0.27$, $N_{agg}$ was 2.3. For this complex, the charged chains were much shorter than the neutral one, and the aggregation number is considerably low. Therefore, we can presume that C03 assumes a star-like conformation[15] rather than core-shell-[16] or core-corona-[17] type micelles. With an increase of $R_p$ up to 1.0, $N_{agg}$ increased. At $R_p = 1.0$, $N_{agg}$ became 30. In the range of $R_p > 1.0$, different results were observed. At $R_p = 4.7$, $N_{gg}$ increased to 70 and at $R_p = 9.5$, $N_{agg}$ reached a magnitude of $10^4$.

### Small angle X-ray scattering

Figure 3 presents the SAXS profiles for all of the samples. For C03, C05 and C10, the exponent $\alpha$ defined by $I(q) \sim q^{\alpha}$ was $\sim 0$ at low $q$, while $\alpha \sim -2$ at high $q$. For C03 and C05, the scattering intensities at

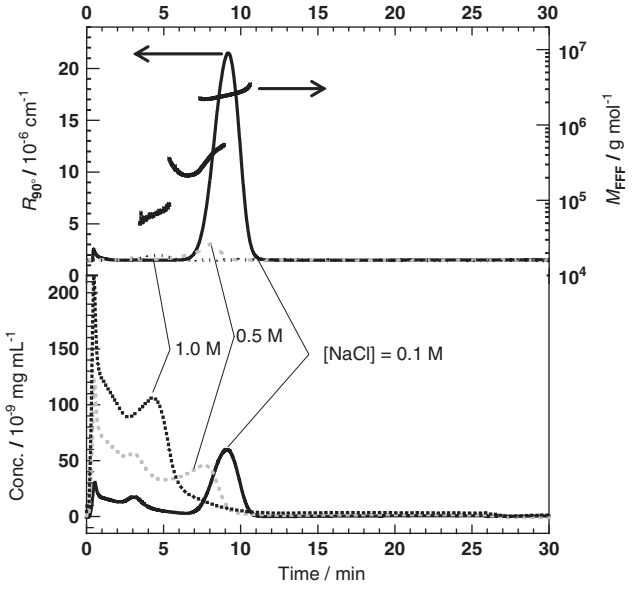


**Figure 2** Fractogram of FFF-multi-angle light scattering (MALS) for C03 in three different salt concentrations. The light-scattering intensity at 90° (upper left), the molar mass for each fraction (upper right) and the concentrations determined from RI (lower).

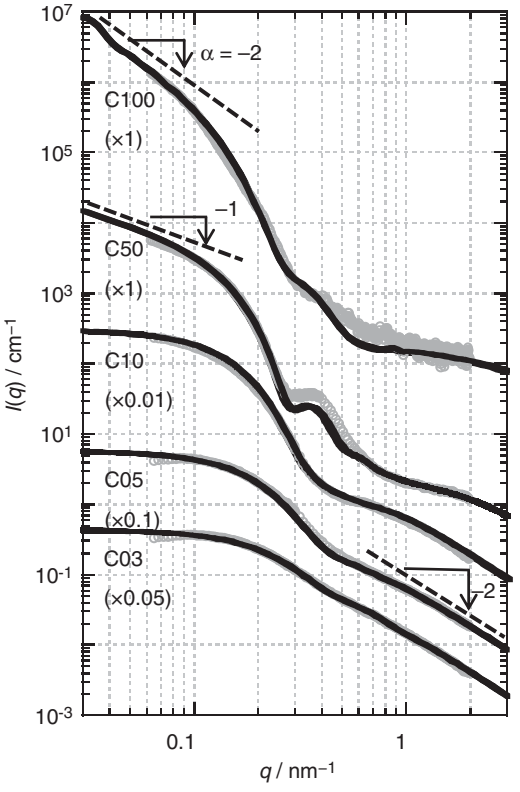


**Figure 3** SAXS profiles and the best-fitted theoretical curves (black lines). For convenience, each curve was vertically shifted by multiplying by the appropriate number in parentheses.

$q < 0.1\,\mathrm{nm}^{-1}$ contained parasitic scattering due to the beam stop. Therefore, we did not use these regions for discussion. With an increase of $R_p$, that is, from C03 to C05, the intensity minimum near $q = 0.35\,\mathrm{nm}^{-1}$ became more obvious and slightly shifted toward lower $q$. For C10, the $q$ dependence of $I(q)$ at both high and low regions were $\alpha \sim 0$ and $\alpha \sim -2$, respectively; however, there was a clear minimum at $q = 0.40\,\mathrm{nm}^{-1}$. The value of $\alpha \sim -2$ is characteristic for the Gaussian chains, which means that the second term in Supplementary Equation 1 dominates at high $q$ for these three samples due to relatively small $N_{agg}$. As described above, this second term can be expressed by the Debye function of Supplementary Equation 3, and its asymptotic behaviors at low-$q$ and high-$q$ are $F_{ch} \sim q^0$ and $\sim q^{-2}$ (see the Supplementary Information), respectively. Therefore, one may suppose that the scattering profiles for these three samples, especially for C03, can be fitted by an equation only consisting of the Debye functions and an appropriate model corresponding to such an expression, for example, star polymers without solid core parts.[18,19] However, such a model cannot rationalize the presence of the intensity minimum at $q = 0.35\,\mathrm{nm}^{-1}$. To reproduce both the intensity minimum and the decay of $I(q) \sim q^{-2}$, we need a Debye function and an additional function that has a larger exponent of $\alpha$, that is, $\alpha < -2$ at high $q$. Thus, we selected Supplementary Equation 4 to fit the data. As $N_{agg}$ is relatively small for C03, C05 and C10, we presumed that this core-corona model is appropriate in terms of physical standpoints. For analyzing the data, we rewrote Supplementary Equation 4 as follows:

$$I(q) = [(\rho_1 - \rho_2)V_1 A_s(q, R_1) + (\rho_2 - \rho_{sol})V_2 A_s(q, R_S)]^2 + N\left[(\rho_2 - \rho_{sol})\frac{V_2 - V_1}{N}\right]^2 F_{Ch}(q, R_g) - \frac{[(\rho_2 - \rho_{sol})V_2 A_s(q, R_2)]^2}{N}. \quad (1)$$

Here, $\rho_1$, $\rho_2$ and $\rho_{sol}$ are the electron density of the core, corona and solvent regions, respectively. For $\rho_{sol}$, we used $334\,\mathrm{e\,nm}^{-3}$ as calculated from the density and composition of the solvent. $V_1$ and $V_2$ are the volumes of the core and core-plus-corona region given by $V_i = 4/3\pi R_i^3$, respectively. When we fit the data to obtain $R_1$, $R_2$ and $R_g$, we used the aggregation number given in Table 2 for $N_{agg}$ and treated $\rho_1$ and $\rho_2$ as adjustable parameters. For the fitting model to make physical sense, we selected the same values of $\rho_1$ and $\rho_2$ for all three samples, and $R_{g,pMPC} < 1/2(R_2 - R_1)$. The best-fitting curves are presented in Figure 3 as solid lines and are compared with the data, and the used-fitting parameters are listed in Table 3. The agreement between experiments and the model is sufficient to conclude that the core-corona micelle model well represents the spherical micellar structures of C03, C05 and C10.

With increasing $R_p$ and thus the increasing $N_{agg}$, the core size increased from 4 to 9 nm. The fully stretched chain lengths of pAMPS were calculated to be 6.2, 12.4 and 24.9 nm, respectively, and these lengths are much longer than the core sizes. This result implies that the polyion pairs are randomly folded in the core, as expected. The values of $R_S - R_C$ are $\sim 6$ nm and the values of $R_{g,pMPC}$ are 3 nm for all the samples. These unchanged corona sizes are consistent with the length of pMPC not changing for all the samples.

The scattering profile for C50 contained a clear secondary peak at $q = 0.4\,\mathrm{nm}^{-1}$, and there was no Guinier region observed in the present $q$ range. These results indicated that the scattering object for C50 was much larger than C10, which is consistent with a large $N_{agg}$, and its local structure was well defined to yield the secondary peak. Yusa *et al.*[12] performed a transmission electron microscopy examination for C50 and observed short worm-like cylinders (see Supplementary Figure 2). Cylindrical objects are consistent with the low-$q$ behavior of SAXS, where the intensity appears to become $I(q) \sim q^{-2}$ at $q < 0.1\,\mathrm{nm}^{-1}$. We fit the data using Supplementary Equation 6 and the resultant parameters are summarized in Table 3.

Yusa *et al.*[12] also performed transmission electron microscopy observations and observed that C100 took a mono-layered vesicle.[20] As the SAXS intensity at low-$q$ appears to asymptotically merge into the line of $I(q) \sim q^{-2}$, the vesicle model is consistent with the SAXS data. To fit the data using Supplementary Equation 5, we need to adjust seven parameters, although some of these parameters are not independent. Fitting with such multiple parameters may not lead to a unique combination of the parameters. We adopted a contrast-matching technique[21] to solve this problem as follows.

### Contrast matching

When we sequentially add a third component that has a relatively large electron density to the solvent and if we can assume that such an addition does not change the micellar structure, the scattering profile dramatically changes even from the same structures[21] because such an addition changes the $\rho$-value for the layer adjacent to the solvent, for the monolayered vesicles described by Supplementary Equation 5, $\rho_2$ and $\rho_4$. As depicted in Figure 4 (right), we need to determine three geometric parameters: $R_1$, the inner diameter of the vesicle; $t_{corona} = R_2 - R_1 = R_4 - R_3$, the thickness of the corona layer; and $t_{core} = R_3 - R_2$, the thickness of the core layer. Among these parameters, there are rules to follow in terms of the chemical structures. The electron densities of bulk PEG and water are known to be $\rho_{PEG} = 370\,\mathrm{e\,nm}^{-3}$ and $\rho_{water} = 334\,\mathrm{e\,nm}^{-3}$, respectively, and thus, $\rho_{sol} = w\rho_{water} + (1 - w)\rho_{PEG}$. Furthermore, we assumed that the added PEG chains did not enter the pMPC domain, and thus, $\rho_{Ch} = 360\,\mathrm{e\,nm}^{-3}$ for all the experiment that have been determined for the other samples.

Figure 4 demonstrates how the scattering profile was changed by the addition of PEG400. On adding PEG to the C100 solution, the secondary peak near $q = 0.3\,\mathrm{nm}^{-1}$ become apparent at 5 and 10 wt%, and then further addition caused the peak to shift to lower angles and become less apparent at 30 wt%. The addition of PEG400

**Table 3 The best-fitting parameters to reproduce the experimental data**

| *Code* | $R_1$/nm | $R_2$/nm | $R_3$/nm | $R_4$/nm | $L$/nm | $\rho_1$/e nm$^{-1}$ | $\rho_2$/e nm$^{-1}$ | $\rho_3$/e nm$^{-1}$ | $\rho_4$/e nm$^{-1}$ | $\sigma/R_S$ | *Model* | d | $R_{g,SAXS}$/nm |
|---|---|---|---|---|---|---|---|---|---|---|---|---|---|
| C03 | 4 | 10.5 | — | — | — | 400 | 344 | — | | 0.20 | Sphere | 0.11 | 6.7 |
| C05 | 5 | 11.5 | — | — | — | 400 | 344 | — | | 0.20 | Sphere | 0.37 | 8.3 |
| C10 | 8.7 | 15.8 | — | — | — | 400 | 344 | — | | 0.25 | Sphere | 0.50 | 12.5 |
| C50 | 13 | 15 | — | — | 100 | 400 | 347 | — | | 0.14 | Cylinder | 0.12 | — |
| C100 | 100 | 104 | 122 | 126 | — | 334 | 360 | 400 | 360 | 0.12 | Vesicle | 1.09 | — |

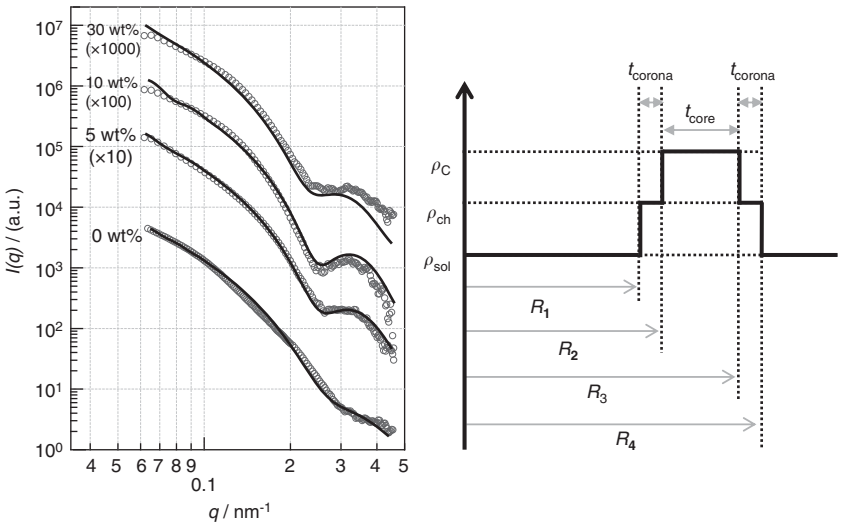


**Figure 4** SAXS profiles of C100 with varying PEG weight fraction at a fixed PIC concentration and theoretical curves of the monolayered vesicle model given by Supplementary equation 5 (solid lines) and a schematic presentation of the electron density profile for the vesicle model.

**Table 4 SAXS fitting parameter for PIC vesicle with contrast variation**

| *PEG conc./wt%* | $t_{corona}$/nm | $\rho_{sol}$/e nm$^{-1}$ | $\sigma/R_1$ |
|---|---|---|---|
| 0 | 21.0 | 334.0 | 0.24 |
| 5 | 22.0 | 336 | 0.16 |
| 10 | 23.5 | 337.5 | 0.13 |
| 15 | 23.0 | 340 | 0.20 |
| 30 | 24.0 | 345.0 | 0.18 |

Abbreviations: PICS, polyion complexes; SAXS, small-angle X-ray scattering.

changed $\rho_{sol}$ from 334 to 345 e nm$^{-3}$ at 30 wt%. For each profile, we attempted to fit all the data using the same parameters, except for $\rho_{sol}$. The resulting theoretical curves are compared with the data in Figure 4, and the obtained parameters are listed in Table 4. The agreement between the values is good, indicating that the monolayered vesicle model is sufficient to describe C100.

The contrast-matching technique has been used commonly in neutron scattering, normally changing the composition of $H_2O$/$D_2O$.[22] In this case, there is almost no risk that changing the solvent composition alters the conformation or structures of the solutes. To do the same in SAXS, we must add a third component to the solvent to change its electron density, which may cause a change in the structures of the solutes. As illustrated in Figure 4 (left), all of the scattering profiles were able to be fitted by the same structural parameters, although the scattering profiles were dramatically changed on adding PEG. This fact ensures that the added PEG did not cause major changes in the structures as well as proving that the obtained parameters were suitable.

### Overcrowding nature of the MPC block

The manner in which the tethered chains are crowding on the flat surface can be described by the chain density ($d$) reduced by the sum of the cross-sectional area of the corona chains per surface area, where $R_g$ is the radius of gyration of the isolated chain at its unperturbed state.[23] When this index is $<4$, the tethered chains are not interacting with each other. When this index is from 4 to 10, the chains cross over with each other and the conformation of each chain deviates from a sphere. In the range of $\sigma > 10$, the chains are more stretched to the direction normal to the surface. Svaneborg and Pedersen[24] extended this concept to the shell of polymeric micelles, and the reduced chain density is given by

$$d = \frac{N_{agg}\pi R_{g,pMPC}^2}{4\pi\left(R_C + R_{g,pMPC}\right)^2}. \quad (2)$$

In this model, each corona chain is assumed to contact at $R_C + R_{g,pMPC}$ from the center of the core. From the same viewpoint, $\sigma$ can be expanded to the surface of cylindrical and unilamellar vesicles:

$$d_{cylinder} = \frac{N_{agg}\pi R_{g,pMPC}^2}{2\pi\left(R_C + R_{g,pMPC}\right)L}, \quad (3)$$

$$d_{vesicle} = \frac{N_{agg}\pi R_{g,pMPC}^2}{4\pi\left(R_{C,in} - R_{g,pMPC}\right)^2 + 4\pi\left(R_{C,out} + R_{g,pMPC}\right)^2}, \quad (4)$$

where $R_{g,pMPC}$ is the radius of gyration of the pMPC single chain; in our case $R_{g,pMPC} = 3$ nm for $M_w \sim 5000$, and $R_{C,in}$ and $R_{C,out}$ are the inner and outer radii of the core of the vesicle, respectively.

We already know all of the parameters needed to determine the surface chain density $d$ given by the three equations. The obtained $d$-values of pMPC are listed in Table 3; these values increased from 0.1 to 1.0 with an increase of $N_{agg}$. Compared with the polymeric micelles composed of PEG hydrophilic blocks, the values of $d$ for C03, C05 and C10 were very small.[25] It can be assumed from $d = 0.11$ for C03 that the pMPC chain was not crowded to completely cover the core. In fact, the graft density of the pMPC on the core surface was $\sim 0.02$ chains per nm$^2$ (this value increased from 0.011 to 0.029 with an increase of $N_{agg}$), which was quite small, compared with $1/R_g^2 \sim 0.06$ nm$^{-2}$. If the core is sufficiently hydrophobic, this less-crowded shell may cause secondary aggregation. The stable micelle formation for the present case can be attributed to the less hydrophobic nature of the core prepared from polyion paring and/or to the chemical nature of MPC, which can be associated with $\sim 24$ water molecules.[9]

## CONCLUSIONS

We performed FFF-MALS and SAXS for five PIC samples with different block lengths. $N_{agg}$ increased from 2.3 to $10^4$ with an increase

of $R_p$ from 0.27 to 9.5. The PIC structures were determined by analyzing the SAXS data using an appropriate model. When $R_p = 0.27$, a star-like spherical conformation was observed. With an increase of $R_p$, the spherical form was maintained up to $R_p = 1.0$, although the conformation transformed from the star to core-corona type. For $R_p = 4.7$, the complex transformed into a worm-like cylinder, and when $R_p = 9.5$ the complex became a vesicle. Based on the determined structural parameters and the aggregation numbers, the crowding parameter ($d$) was determined. For all of the samples, $d$ was much smaller than that of PEG.

## ACKNOWLEDGEMENTS

This work was financially supported by the JST CREST program and all the SAXS measurements were performed at SPring-8 40B2 (2011B1735, 2012A1218, 2012B1252, 2012B1662, 2013A1207 and 2013A1594).

1 Tsuchida, E., Abe, K. & Honma, M. Aggregation of polyion complexes between synthetic polyelectrolytes. *Macromolecules* **9,** 112–117 (1976).
2 Pergushov, D. V., Muller, A. H. E. & Schacher, F. H. Micellar interpolyelectrolyte complexes. *Chem. Soc. Rev.* **41,** 6888–6901 (2012).
3 Harada, A. & Kataoka, K. Chain length recognition: core-shell supramolecular assembly from oppositely charged block copolymers. *Science* **283,** 65–67 (1999).
4 Hamley, I. W. *The Physics of Block Copolymers* (Oxford University Press, 1998).
5 Kataoka, K., Harada, A. & Nagasaki, Y. Block copolymer micelles for drug delivery: design, characterization and biological significance. *Adv. Drug Deliv. Rev.* **47,** 113–131 (2001).
6 Amiji, M. & Park, K. Prevention of protein adsorption and platelet adhesion on surfaces by PEO/PPO/PEO triblock copolymers. *Biomaterials* **13,** 682–692 (1992).
7 Ishida, T., Ichikawa, T., Ichihara, M., Sadzuka, Y. & Kiwada, H. Effect of the physicochemical properties of initially injected liposomes on the clearance of subsequently injected PEGylated liposomes in mice. *J. Controlled Release* **95,** 403–412 (2004).
8 Ishida, T., Harada, M., Wang, X. Y., Ichihara, M., Irimura, K. & Kiwada, H. Accelerated blood clearance of PEGylated liposomes following preceding liposome injection: effects of lipid dose and PEG surface-density and chain length of the first-dose liposomes. *J. Controlled Release* **105,** 305–317 (2005).
9 Sugihara, S., Blanazs, A., Armes, S. P., Ryan, A. J. & Lewis, A. L. Aqueous dispersion polymerization: a new paradigm for in situ block copolymer self-assembly in concentrated solution. *J. Am. Chem. Soc.* **133,** 15707–15713 (2011).
10 Morisaku, T., Watanabe, J., Konno, T., Takai, M. & Ishihara, K. Hydration of phosphorylcholine groups attached to highly swollen polymer hydrogels studied by thermal analysis. *Polymer (Guildf)* **49,** 4652–4657 (2008).
11 Yusa, S.-i., Yokoyama, Y. & Morishima, Y. Synthesis of oppositely charged block copolymers of poly(ethylene glycol) via reversible addition−fragmentation chain transfer radical polymerization and characterization of their polyion complex micelles in water. *Macromolecules* **42,** 376–383 (2008).
12 Nakai, K., Nishiuchi, M., Inoue, M., Ishihara, K., Sanada, Y., Sakurai, K. & Yusa, S. i. – Preparation and characterization of polyion complex micelles with phosphobetaine shells. *Langmuir* **29,** 9651–9661 (2013).
13 Fujisawa, T., Inoue, K., Oka, T., Iwamoto, H., Uruga, T., Kumasaka, T., Inoko, Y., Yagi, N., Yamamoto, M. & Ueki, T. Small-angle X-ray scattering station at the SPring-8 RIKEN beamline. *J. Appl. Crystallogr.* **33,** 797–800 (2000).
14 Masunaga, H., Ogawa, H., Takano, T., Sasaki, S., Goto, S., Tanaka, T., Seike, T., Takahashi, S., Takeshita, K., Nariyama, N., Ohashi, H., Ohata, T., Furukawa, Y., Matsushita, T., Ishizawa, Y., Yagi, N., Takata, M., Kitamura, H., Sakurai, K., Tashiro, K., Takahara, A., Amamiya, Y., Horie, K., Takenaka, M., Kanaya, T., Jinnai, H., Okuda, H., Akiba, I., Takahashi, I., Yamamoto, K., Hikosaka, M., Sakurai, S., Shinohara, Y., Okada, A. & Sugihara, Y. Multipurpose soft-material SAXS/WAXS/GISAXS beamline at SPring-8. *Polymer J.* **43,** 471–477 (2011).
15 Daoud, D. & Cotton, J. P. Star shaped polymers:a model for the conformation and its concentration dependence. *J. Phys.* **43,** 531–538 (1982).
16 Nakano, M., Matsuoka, H., Yamaoka, H., Poppe, A. & Richter, D. Sphere to rod transition of micelles formed by amphiphilic diblock copolymers of vinyl ethers in aqueous solution. *Macromolecules* **32,** 697–703 (1999).
17 De Santis, S., Diana Ladogana, R., Diociaiuti, M. & Masci, G. Pegylated and thermosensitive polyion complex micelles by self-assembly of two oppositely and permanently charged diblock copolymers. *Macromolecules* **43,** 1992–2001 (2010).
18 Pedersen, J. S. Structure factors effects in small-angle scattering from block copolymer micelles and star polymers. *J. Chem. Phys.* **114,** 2839–2846 (2001).
19 Castelletto, V. & Hamley, I. Small-angle scattering functions of micelles. *Fibre Diffract. Rev.* **11,** 36–43 (2003).
20 Nakai, K., Ishihara, K. & Yusa, S. Polyion complex vesicles covered with phosphorylcholine groups. *Polym. Prep. Jpn* **62,** 522 (2013).
21 Naruse, K., Eguchi, K., Akiba, I., Sakurai, K., Masunaga, H., Ogawa, H. & Fossey, J. S. Flexibility and cross-sectional structure of an anionic dual-surfactant wormlike micelle explored with small-angle X-ray scattering coupled with contrast variation technique. *J. Phys. Chem. B* **113,** 10222–10229 (2009).
22 Potschke, D., Ballauff, M., Lindner, P., Fischer, M. & Vogtle, F. Analysis of the structure of dendrimers in solution by small-angle neutron scattering including contrast variation. *Macromolecules* **32,** 4079–4087 (1999).
23 Chen, W. Y., Zheng, J. X., Cheng, S. Z. D., Li, C. Y., Huang, P., Zhu, L., Xiong, H., Ge, Q., Guo, Y., Quirk, R. P., Lotz, B., Deng, L., Wu, C. & Thomas, E. L. Onset of Tethered Chain Overcrowding. *Phys. Rev. Lett.* **93,** 028301 (2004).
24 Svaneborg, C. & Pedersen, J. S. Form factors of block copolymer micelles with excluded-volume interactions of the corona chains determined by monte carlo simulations. *Macromolecules* **35,** 1028–1037 (2001).
25 Sanada, Y., Akiba, I., Sakurai, K., Shiraishi, K., Yokoyama, M., Mylonas, E., Ohta, N., Yagi, N., Shinohara, Y. & Amemiya, Y. Hydrophobic molecules infiltrating into the poly(ethylene glycol) domain of the core/shell interface of a polymeric micelle: evidence obtained with anomalous small-angle X-ray scattering. *J. Am. Chem. Soc.* **135,** 2574–2582 (2013).

Supplementary Information accompanies the paper on Polymer Journal website (http://www.nature.com/pj)